Phys. Med. Biol. **44** (1999) 1543–1563. Printed in the UK PII: S0031-9155(99)98521-4

Non-invasive optical monitoring of the newborn piglet brain using continuous-wave and frequency-domain spectroscopy

Sergio Fantini†, Dennis Hueber‡, Maria Angela Franceschini†, Enrico Gratton†, Warren Rosenfeld§, Phillip G Stubblefield‖, Dev Maulik§ and Miljan R Stankovic§‖

† Laboratory for Fluorescence Dynamics, Department of Physics, University of Illinois at Urbana-Champaign, 1110 West Green Street, Urbana, IL 61801-3080, USA
‡ ISS, Incorporated, 2604 North Mattis Avenue, Champaign, IL 61821, USA
§ Departments of Obstetrics/Gynecology and Pediatrics, Winthrop University Hospital, State University of New York, Stony Brook School of Medicine, 259 First Street, Mineola, NY 11501, USA
‖ Department of Obstetrics and Gynecology, Boston University School of Medicine, 1 Boston Medical Center Place, Boston, MA 02118, USA

Received 20 October 1998, in final form 1 March 1999

Abstract. We have used continuous-wave (CW) and frequency-domain spectroscopy to investigate the optical properties of the newborn piglet brain *in vivo* and non-invasively. Three anaesthetized, intubated, ventilated and instrumented newborn piglets were placed into a stereotaxic instrument for optimal experimental stability, reproducible probe-to-scalp optical contact and 3D adjustment of the optical probe. By measuring the absolute values of the brain absorption and reduced scattering coefficients at two wavelengths (758 and 830 nm), frequency-domain spectroscopy provided absolute readings (in contrast to the relative readings of CW spectroscopy) of cerebral haemoglobin concentration and saturation during experimentally induced perturbations in cerebral haemodynamics and oxygenation. Such perturbations included a modulation of the inspired oxygen concentration, transient brain asphyxia, carotid artery occlusion and terminal brain asphyxia. The baseline cerebral haemoglobin saturation and concentration, measured with frequency-domain spectroscopy, were about 60% and 42 μM respectively. The cerebral saturation values ranged from a minimum of 17% (during transient brain asphyxia) to a maximum of 80% (during recovery from transient brain asphyxia). To analyse the CW optical data, we have (a) derived a mathematical relationship between the cerebral optical properties and the differential pathlength factor and (b) introduced a method based on the spatial dependence of the detected intensity (dc slope method). The analysis of the cerebral optical signals associated with the arterial pulse and with respiration demonstrates that motion artefacts can significantly affect the intensity recorded from a single optode pair. Motion artefacts can be strongly reduced by combining data from multiple optodes to provide relative readings in the dc slope method. We also report significant biphasic changes (initial decrease and successive increase) in the reduced scattering coefficient measured in the brain after the piglet had been sacrificed.

1. Introduction

Near-infrared spectroscopy is a non-invasive monitoring technique that can probe living tissues to a depth of the order of centimetres. The optical parameters of tissues, namely the absorption and the reduced scattering coefficients, are representative of the physiological state and in particular of the haemoglobin concentration and saturation. Recent applications of non-invasive tissue spectroscopy in the skeletal muscles include the optical monitoring of the

0031-9155/99/061543+21$19.50

oxygenation during ischaemia (Hampson and Piantadosi 1988, Ferrari *et al* 1992, Sahlin 1992, Fantini *et al* 1995, Miwa *et al* 1995) or exercise (Chance *et al* 1992, Belardinelli *et al* 1995, Hamaoka *et al* 1996, Franceschini *et al* 1997, Quaresima *et al* 1998), the assessment of the local blood flow and oxygen consumption (Edwards *et al* 1993, De Blasi *et al* 1993, 1994, Homma *et al* 1996) and the diagnosis of claudication (Cheatle *et al* 1991, McCully *et al* 1994, Kooijman *et al* 1997, Franceschini *et al* 1998a). Near-infrared spectroscopy has also been non-invasively applied to the human infant's brain to measure cerebral oxygenation and hemodynamics (Cope and Delpy 1988, Edwards *et al* 1988) and in adults to quantify cerebral hemodynamics (Elwell *et al* 1994), to monitor brain activity (Gratton *et al* 1995, Meek *et al* 1995, Wenzel *et al* 1996, Tamura *et al* 1997, Villringer and Chance 1997) and to detect intracranial haematomas (Gopinath *et al* 1993, Hennes *et al* 1999). To test the results provided by cerebral tissue spectroscopy, validation studies on the piglet brain have been performed using CW (Brun *et al* 1997, Stankovic *et al* 1998), frequency-domain (Du *et al* 1998) and time-domain (Yamashita *et al* 1996) spectroscopy.

In this article, we report non-invasive measurements on the newborn piglet brain performed with frequency-domain spectroscopy. This technique affords the absolute measurement of the tissue absorption and reduced scattering coefficients, as well as the tissue haemoglobin concentration and saturation. Our instrument also acquires the average intensity, which is the measured parameter in CW spectroscopy, so that we can compare the frequency-domain and the CW approaches to tissue spectroscopy. To investigate the information content and the sensitivity of near-infrared cerebral spectroscopy, we have optically monitored the temporal evolution of the haemoglobin concentration and saturation during various manipulations to the cerebral blood flow and/or oxygen supply. Furthermore, by using an acquisition time of 160 ms, we have examined the optical signals associated with the arterial pulse and with respiration, to investigate whether their origin is physiological or related to motion artefacts.

2. Experimental and theoretical methods

2.1. Animal preparation

The animals used in this study were maintained in accordance with the guidelines of the Winthrop University Hospital Animal Use Committee and the *Guide for the Care and Use of Laboratory Animals* by the Institute of Laboratory Animal Resources, National Research Council (NIH Guide, volume 25, no 28, 16 August 1996). Optical measurements were performed in three newborn piglets (11 ± 1 days old; weight: 2.7 ± 0.6 kg) which we labelled with the letters A, B and C. The piglets were sedated with ketamine (25–30 mg kg^{-1} IM) and anaesthetized by the infusion of propofol and sodium pentobarbital. The piglets were intubated and ventilated by a paediatric ventilator (Bear CUB Infant Ventilator, Bear Medical Systems, Inc., Riverside, CA) which allowed us to vary the ventilated oxygen per cent from 21 to 100%. The ventilation was adjusted to maintain the desired values of arterial blood gases. A pulse oximeter (Nellcor PM-1000, Nellcor Inc., Hayward, CA) was used to monitor the heart rate by attaching its probe to the tail of the piglet. Body temperature was maintained at 37 °C with a warming blanket. Right femoral cut-down was performed to insert the catheters into the abdominal aorta for continuous mean arterial blood pressure measurements (Hewlett Packard 78353B, USA) and for intermittent arterial blood gas measurements (Corning 238, pH blood gas analyser, Ciba, Medfield, MA) and into the inferior vena cava for the infusion of propofol/pentobarbital anaesthesia and hydration. The pre-shaved head of the animal was placed into a stereotaxic instrument (Lab Standard 51600, Stoelting, Wood Dale, IL) in order to provide mechanical stability, optimal optical coupling and 3D positioning capability for the optical probe.

2.2. Experimental procedure

After a period of stabilization, we recorded mean arterial blood pressure, heart rate and arterial blood gases, pH and oxygen saturation. The piglets underwent four different experimental protocols, which are described in sections 2.2.1 to 2.2.4. To verify the reproducibility of our measurements, some of the experiments were conducted more than once. Optical measurements were compared with conventional measurements of arterial oxygen saturation and heart rate. At the end of the first three experimental protocols, the animals recovered spontaneously and no resuscitation was required.

2.2.1. Modulation of the inspired oxygen concentration. Piglet A was subjected to changes in the inspired oxygen concentration. The concentration of the inspired oxygen was reduced in a stepwise fashion, by 20% every 2 min, from the initial value of 100%, all the way down to 21% (the room air oxygen concentration) and then it was increased back to the initial value of 100% by increments of 20% every 2 min. Arterial blood was drawn to measure arterial oxygen saturation at the end of each particular step, i.e. before the transition to the next oxygen level.

2.2.2. Transient brain asphyxia. After the experiment described in section 2.2.1, piglet A was subjected to a transient 3.2 min episode of asphyxia induced by turning the respirator off. This type of experiment has been previously described in newborn piglets (Stankovic *et al* 1998). Arterial oxygen saturation was sampled before, during and after peak response.

2.2.3. Carotid artery occlusion. Piglet B was placed in a supine position (i.e. lying on its back), with the optical probe positioned underneath the left side of the piglet's head. Surgery was performed to expose both the right and left common carotid arteries. Using small vascular clamps, either one or both carotid arteries were occluded, with the purpose of investigating the capability of near-infrared spectroscopy to detect and quantify the occlusion-induced changes in cerebral blood oxygenation.

2.2.4. Terminal brain asphyxia. At the end of the study, all three piglets were sacrificed by an overdose of sodium pentobarbital (500 mg IV). Sodium pentobarbital induces cardiac arrest, the cessation of cerebral blood flow and terminal brain asphyxia, followed by cell death as a consequence of hypoxia. Terminal brain asphyxia appeared to be a valuable source of optical information that we decided to report in this manuscript.

2.3. Absolute measurements with frequency-domain spectroscopy

The optical study has been performed with a frequency-domain (110 MHz) tissue spectrometer (Franceschini *et al* 1997) operating at two near-infrared wavelengths, namely 758 and 830 nm (tissue oximeter model 96208, ISS, Inc., Champaign, IL). This instrument allows for the determination of the average value (dc), amplitude (ac) and phase (Φ) of the modulated intensity at four different source–detector distances at each wavelength. This multidistance method affords the quantitative assessment of the absorption (μ_a) and reduced scattering (μ_s') coefficients of tissues by the use of either the (dc, Φ) or (ac, Φ) pair of data (Fantini *et al* 1994a). In this study, we have used the (ac, Φ) pair to minimize the effect, mostly on the dc readings, of possible leakage of room light into the optical probe. If we denote with S_{ac} and S_Φ, respectively, the slopes of $\ln(r^2\mathrm{ac})$ and Φ as a function of r, the absolute values of μ_a and

μ_s' of a semi-infinite medium in the diffusion approximation are given by (Fantini *et al* 1994a)

$$\mu_a = \frac{\omega}{2v}\left(\frac{S_\Phi}{S_{\rm ac}} - \frac{S_{\rm ac}}{S_\Phi}\right) \tag{1}$$

$$\mu_s' = \frac{S_{\rm ac}^2 - S_\Phi^2}{3\mu_a} - \mu_a \tag{2}$$

where ω is the angular modulation frequency of the source intensity and v is the speed of light in the tissue. The slope of $\ln(r^2{\rm ac})$ approximates the slope of a more complicated function of r, ac, μ_a and μ_s' (Fantini *et al* 1994b). This is an excellent approximation when $r\sqrt{3\mu_a\mu_s'} \gg 1$. In our measurements, the quantity $r\sqrt{3\mu_a\mu_s'}$ typically ranged between 3 and 6. The source–detector distances were 1.5, 2.0, 2.5 and 3.0 cm to achieve a mean optical penetration depth of the order of 0.5 cm (Patterson *et al* 1995). This optical penetration depth is sufficient to non-invasively probe the piglet brain, since the outer skin/scalp/skull layer has an overall thickness of about 0.4 cm as measured post mortem. We have recently shown, by experiments on phantoms, that the frequency-domain multidistance method carried out at distances larger than 1.5 cm is not affected by the presence of a superficial layer having a thickness less than or equal to 0.4 cm (Franceschini *et al* 1998b). Therefore, our optical probe should actually measure the brain optical properties. We note, however, that the strong tissue inhomogeneity encountered in non-invasive brain spectroscopy (skin, scalp, skull, dura, cerebrospinal fluid, convolutions of the brain, etc) may affect the accuracy of absolute measurements. The quantitative measurement of the tissue absorption at two near-infrared wavelengths can be translated into a quantitative reading of haemoglobin concentration and saturation, by taking advantage of the different absorption spectra of oxy- and deoxyhaemoglobin (Millikan 1942, Eaton *et al* 1978, Sevick *et al* 1991, Fantini *et al* 1995). As a result, one obtains the concentration and saturation of haemoglobin in the tissue, so that the arterial, venous and capillary components will all contribute to the measurement. It has been shown that the main contribution to tissue spectroscopy comes from the haemoglobin in the smaller blood vessels (Liu *et al* 1995a).

The eight 400 μm source optical fibres (four guiding light at 758 nm, four at 830 nm) and the 3 mm detector fibre bundle were positioned on the piglet head as shown in figure 1. The source–detector line, which was parallel to the sagittal sinus, was centred on the head of piglet A, whereas it was displaced from the centre by 1 cm to the left (right) in piglet B (C). The detector fibre was passed through a black metal plate held at a distance of about 0.6 cm from the piglet head (see figure 1). This distance enabled us to visually inspect the optical coupling between the optical fibres and the piglet head. The tip of the detector fibre was placed in good contact with the head of the piglet. The source fibres were free to slide in snug holes drilled in the black plate until the fibre tips came in contact with the skin. All the fibres were fixed to a post to keep them bent in such a way that they exerted a slight pressure on the skin (see figure 1). In this fashion, we achieved a good optical contact on the skin, preventing the fibres from retracting away from the piglet head, while maintaining the flexibility required to adapt the optical probe to the curved surface of the piglet head. The black plate and the post were rigidly attached to the stereotaxic instrument on which three knobs allowed the 3D positioning of the probe. A light block was inserted between the source and the detector fibres to prevent any light from reaching the detector without travelling inside the head. Additional light blocks were wrapped around the optical probe to cut room light. The eight laser diodes were multiplexed at a rate of 50 Hz, so that only one light source was on (for 20 ms) at a time. The acquisition time per cycle over the eight light sources was 160 ms, i.e. 8 diodes$\times$20 ms/diode. In piglets A and B, we averaged eight cycles to get an overall acquisition time of 1.28 s, which was sufficient to monitor the relatively slow dynamic

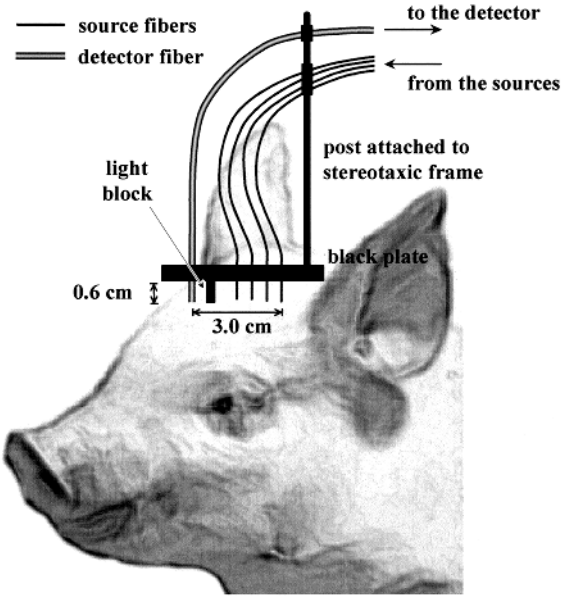

Figure 1. Arrangement of the optical probe on the piglet head. The source optical fibres are free to slide through snug holes in the black plate and they are bent to exert a slight pressure on the skin.

processes resulting from haemodynamics and modifications to the oxygen supply. In piglet C, we considered only one cycle per data point to achieve an actual acquisition time of 160 ms. This latter acquisition rate is faster than the heart rate, thereby allowing for optical monitoring of cerebral arterial pulsations, as well as slower respiration-associated changes.

2.4. Relative measurements using the average intensity (continuous wave spectroscopy)

The frequency-domain spectrometer also acquires continuous wave (CW) intensity data (the dc signal), which can be used to quantify the changes in the absorption coefficient. These changes can be translated into changes in the concentrations of oxy- and deoxyhaemoglobin. To this aim, one can follow two approaches: the differential pathlength factor (DPF) method, or the dc slope method (which also affords absolute measurements).

2.4.1. Differential pathlength factor (DPF). The DPF method has been widely used in CW tissue spectroscopy to quantify changes in the concentration of tissue chromophores (Cope *et al* 1991, Edwards *et al* 1993, Meek *et al* 1995, Stankovic *et al* 1998). The DPF is a parameter that takes into account the increased photon pathlength caused by multiple light scattering in tissues (Delpy *et al* 1988, Cope *et al* 1991). Under the assumptions that the reduced scattering coefficient μ_s' remains constant and that the absorption coefficient μ_a does not vary by a large amount (variations small with respect to μ_a), the change in the absorption coefficient ($\Delta\mu_a(t)$) at time t with respect to time 0 can be written as

$$\Delta\mu_a(t) = \frac{1}{r\mathrm{DPF}} \ln\left(\frac{\mathrm{dc}(0)}{\mathrm{dc}(t)}\right) \tag{3}$$

where r is the source–detector distance, while (dc)(0) and (dc)(t) are the dc intensities measured at time 0 and time t respectively. The value of the DPF is usually taken from published values

measured on similar tissues with time-resolved methods. Since there are no published DPF values for the piglet brain, previous studies on piglets have assumed values of 3.85 (Brun *et al* 1997) or 4.39 (Stankovic *et al* 1998), which are values reported for the brain of newborn infants (Wyatt *et al* 1990, Van der Zee *et al* 1992).

The relationship between the DPF and the tissue optical coefficients μ_a and μ_s' can be found by using diffusion theory. In an infinite turbid medium, diffusion theory and equation (3) yield the following relationship:

$$\mathrm{DPF}_{\mathrm{inf}} = \frac{\sqrt{3\mu_s'}}{2\sqrt{\mu_{a0}}}. \tag{4}$$

In the semi-infinite geometry, the dc intensity predicted by diffusion theory is the following (Farrel *et al* 1992, Fantini *et al* 1994b, Liu *et al* 1995b):

$$\mathrm{dc}_{\mathrm{seminf}}(0) = C\frac{\mathrm{e}^{-\sqrt{3\mu_{a0}\mu_s'}r}}{r^2}\left(\sqrt{3\mu_{a0}\mu_s'} + \frac{1}{r}\right) \tag{5}$$

$$\mathrm{dc}_{\mathrm{seminf}}(t) = C\frac{\mathrm{e}^{-\sqrt{3(\mu_{a0}+\Delta\mu_a)\mu_s'}r}}{r^2}\left(\sqrt{3(\mu_{a0}+\Delta\mu_a)\mu_s'} + \frac{1}{r}\right) \tag{6}$$

where C is a proportionality factor, μ_s' is assumed to be constant, μ_{a0} is the absorption coefficient at time 0 and the absorption coefficient at time t is written $\mu_a(t) = \mu_{a0} + \Delta\mu_a$ with $\Delta\mu_a/\mu_{a0} \ll 1$. By dividing equation (5) by equation (6) and assuming that $\Delta\mu_a/\mu_{a0} \ll 1$, after some algebra one finds

$$\Delta\mu_a \approx \frac{2\sqrt{\mu_{a0}}}{\sqrt{3\mu_s'}r}\frac{r\sqrt{3\mu_{a0}\mu_s'}+1}{r\sqrt{3\mu_{a0}\mu_s'}}\ln\left(\frac{\mathrm{dc}_{\mathrm{seminf}}(0)}{\mathrm{dc}_{\mathrm{seminf}}(t)}\right) \tag{7}$$

which, after comparison with equation (3), gives

$$\mathrm{DPF}_{\mathrm{seminf}} = \frac{\sqrt{3\mu_s'}}{2\sqrt{\mu_{a0}}}\frac{r\sqrt{3\mu_{a0}\mu_s'}}{r\sqrt{3\mu_{a0}\mu_s'}+1}. \tag{8}$$

This approach to finding the DPF is equivalent to the definition (Cope *et al* 1991, Arridge *et al* 1992)

$$\mathrm{DPF} \equiv \frac{1}{r}\frac{\partial A}{\partial \mu_a}\bigg|_{\mu_{a0}} \tag{9}$$

where A is the optical attenuation defined as $\ln(\mathrm{dc}(0)/\mathrm{dc}(t))$. It is interesting to note that the same result can be found by using an alternative definition of the DPF (namely, the ratio of the average photon pathlength $\langle L\rangle$ to the source–detector distance r) (Essenpreis *et al* 1993) and the Green function for the diffusion equation in the semi-infinite geometry:

$$\mathrm{DPF}_{\mathrm{seminf}} \equiv \frac{\langle L\rangle}{r} \simeq \frac{v\langle t\rangle}{r} = \frac{v}{r}\frac{\int_0^\infty tG_{\mathrm{seminf}}(r,t)\,\mathrm{d}t}{\int_0^\infty G_{\mathrm{seminf}}(r,t)\,\mathrm{d}t} = \frac{\sqrt{3\mu_s'}}{2\sqrt{\mu_{a0}}}\frac{r\sqrt{3\mu_{a0}\mu_s'}}{r\sqrt{3\mu_{a0}\mu_s'}+1} \tag{10}$$

where $\langle t\rangle$ is the average photon time of flight and the semi-infinite medium Green function $G_{\mathrm{seminf}}(r,t)$ is $\propto t^{-5/2}\exp[-3\mu_s'r^2/(4vt) - \mu_a vt]$ (Patterson *et al* 1989).

We point out two important results:

(a) The relationship between the DPF and the optical coefficients is different in the infinite and semi-infinite geometries, which means that in a given material we have $\mathrm{DPF}_{\mathrm{inf}} \neq \mathrm{DPF}_{\mathrm{seminf}}$. Obviously, the semi-infinite geometry is a better model for non-invasive diffused-reflectance spectroscopy.

(b) In the semi-infinite geometry, $\mathrm{DPF}_{\mathrm{seminf}}$ increases with source–detector distance r and reaches the asymptotic value of $\mathrm{DPF}_{\mathrm{inf}}$ when $r\sqrt{3\mu_{a0}\mu_s'} \gg 1$.

For typical optical properties of tissues, this latter condition requires that r be much greater than 0.5–0.7 cm. It has been reported that the DPF measured *in vivo* is approximately constant at source–detector distances larger than about 3.0 cm (Van der Zee *et al* 1992).

2.4.2. Slope of ln(r^2dc) versus source–detector distance r (dc slope). Equation (5) shows that in the limit $r\sqrt{3\mu_a\mu_s'} \gg 1$, the $\ln(r^2\mathrm{dc}_{\mathrm{seminf}})$ is a linear function of r, which has a slope $S_{\mathrm{dc}} = -\sqrt{3\mu_a\mu_s'}$ (Liu *et al* 1995b). By assuming a constant value for μ_s', the absolute value of μ_a (and consequently also the variations in μ_a) can be quantified by the following expression:

$$\mu_a = \frac{S_{\mathrm{dc}}^2}{3\mu_s'}. \tag{11}$$

We observe that the dc slope method differs from the DPF method in two important respects: (a) it does not require the changes in μ_a to be small; (b) it measures the absolute value of μ_a. As we will see in section 3.5, the dc slope method is also affected by motion artefacts to a lesser extent than the DPF method. However, the condition $r\sqrt{3\mu_a\mu_s'} \gg 1$ implies that, for typical tissue optical properties $\mu_a \sim 0.1$ cm^{-1} and $\mu_s' \sim 10$ cm^{-1}, the dc slope method is more accurate at source–detector distances greater than 1.5–2.0 cm.

2.5. Optical monitoring of arterial pulsation and respiration

Near-infrared spectroscopy can monitor rhythmical physiological phenomena associated with arterial pulse (Franceschini *et al* 1994, Kohl *et al* 1998) and breathing. For instance, pulse oximetry measures the arterial saturation by comparing the pulsatile components recorded at two different wavelengths (Mendelson 1992). In piglet C, we used an acquisition time of 160 ms per point in order to investigate the optical signals related to the heartbeat and respiration. In particular, our objective was to assess the effect of arterial pulsation and respiration on different optical parameters such as the dc intensity, the dc slope (as defined in section 2.4.2) and the phase. We have recorded the optical signal under three different conditions:

(a) piglet alive, ventilator working;
(b) piglet dead, ventilator still working;
(c) piglet dead, ventilator off.

We also recorded the airway pressure by connecting the proximal airway pressure output (analogue output) of the ventilator to an auxiliary input interface system (ISS, Inc., Champaign, IL) connected to the tissue spectrometer. This approach provided synchronous recordings of the optical signal and of the airway pressure. By keeping the ventilator working after the death of the pig, we can investigate whether the optical oscillations recorded by near-infrared spectroscopy in living animals are associated with ventilation-related physiological phenomena (brain perfusion changes), or rather to ventilation-induced motion artefacts.

3. Results

3.1. Optical properties and DPF values

We have not used DPF values reported in the literature. We have measured the optical properties of the piglet brain by frequency-domain spectroscopy and we have obtained the DPF by applying the relationship between the optical properties of a semi-infinite medium and the

Table 1. Optical properties and DPF values measured on the brain of the three piglets under normoxia conditions. The numbers in parentheses are the errors in the last digit of the corresponding value. These errors are mostly determined by limitations in the reproducibility of the optical contact between the optical probe and the piglet head (see table 2).

Wavelength (nm)	Piglet	μ_a (cm^{-1})	μ_s' (cm^{-1})	DPF				
				$r = 1.5$ cm	$r = 2.0$ cm	$r = 2.5$ cm	$r = 3.0$ cm	$r \gg (3\mu_a\mu_s')^{-1/2}$
758	A	0.135(7)	9.7(4)	5.5(3)	5.9(4)	6.1(4)	6.3(5)	7.3(3)
	B	0.145(7)	8.9(4)	5.1(3)	5.4(3)	5.6(4)	5.8(4)	6.8(3)
	C	0.168(7)	9.1(4)	4.9(2)	5.2(3)	5.4(3)	5.5(3)	6.4(3)
830	A	0.110(7)	8.4(4)	5.4(4)	5.8(5)	6.1(5)	6.3(6)	7.6(4)
	B	0.120(7)	7.7(4)	4.9(3)	5.3(4)	5.6(4)	5.8(5)	6.9(4)
	C	0.150(7)	8.7(4)	4.9(3)	5.3(3)	5.5(3)	5.6(4)	6.6(3)

DPF (equation (8)). The baseline values (normoxia condition) of the absorption and reduced scattering coefficients measured with the frequency-domain multidistance method are reported in table 1 for the three piglets at both wavelengths. These values of μ_a and μ_s' are in good agreement with the values measured by Yamashita *et al* (1996) with time-domain spectroscopy at 760 nm. By applying equation (8), using the measured values of μ_a and μ_s', we have obtained the values of DPF_{seminf} for the three piglet brains. These DPF values are reported in table 1 for the four source–detector distances employed by us and also for the limiting case of large distances. We note that the DPF values measured by us are greater than those employed in Brun *et al* (1997) (3.85) and in Stankovic *et al* (1998) (4.39) for the piglet brain.

3.2. Precision and reproducibility of the optical measurements

We assessed the reproducibility (for successive repositioning of the optical probe on the same spot) and the precision (as determined by the instrumental noise and by physiological fluctuations) of our optical measurements at two acquisition times, 1.28 s and 0.16 s. The results are listed in table 2. The reproducibility errors estimate the uncertainty in the absolute readings, whereas the precision gives an indication of the smallest detectable change in the corresponding parameter. The modifications in the optical fibre/skin coupling at each repositioning of the optical probe account for the fact that reproducibility errors are typically one order of magnitude larger than the uncertainty due to precision. Such modifications in the optical coupling are due to a lack of reproducibility in the fibre-to-skin contact and to the presence of hair that may affect the optical coupling in an unpredictable way (the shaved piglet head still had hair about 1 mm long). It is noteworthy that the phase is the only parameter almost unaffected by successive repositioning of the probe (in fact, the reproducibility errors and the precision are comparable). This result shows the low sensitivity of the phase to the fibre-to-skin optical coupling. We observe that the precision in the dc intensity and ac amplitude is not limited by the instrumental noise, but rather by the physiological fluctuations related to the arterial pulse and respiration (see section 3.7).

3.3. Modulation of the inspired oxygen concentration

Figure 2 shows the time traces of cerebral total haemoglobin concentration (THC = $[HbO_2] + [Hb]$) and haemoglobin saturation (Y) in response to a mild reduction in the arterial oxygen saturation. Cerebral haemoglobin saturation, measured with frequency-domain spectroscopy, decreased from $56.5 \pm 0.5\%$ (at 100% oxygen) to $51.5 \pm 0.5\%$ (at 21% oxygen). This 5% decrease in cerebral haemoglobin saturation (as detected by near-infrared spectroscopy)

Table 2. Reproducibility and precision of the optical measurements performed with acquisition times (AT) of 1.28 and 0.16 s. Reproducibility is based on the maximum difference in the parameters as a result of repeated repositioning of the optical probe. Precision is the peak-to-peak fluctuation in the parameters observed with the optical probe fixed on the piglet head. We note that the precision of the dc intensity and ac amplitude is significantly better when the optical probe is placed on a synthetic phantom. This means that the precision of the dc and ac reported in the table is not limited by instrumental noise, but it is rather determined by physiological fluctuations.

Quantity	Reproducibility of absolute measurements (for successive repositioning of the optical probe)	Precision of relative measurements (by keeping the optical probe on the same location)	
		AT = 1.28 s	AT = 0.16 s
dc intensity	15%	0.1%	0.2%
ac amplitude	15%	0.2%	0.3%
Phase	0.15°	0.05°	0.15°
μ_a	0.007 cm^{-1}	0.0005 cm^{-1}	0.005 cm^{-1}
μ_s'	0.4 cm^{-1}	0.03 cm^{-1}	0.3 cm^{-1}
$[HbO_2]$	3 μM	0.3 μM	3 μM
[Hb]	3 μM	0.3 μM	3 μM
THC	3 μM	0.3 μM	2 μM
Y	6%	0.5%	4%

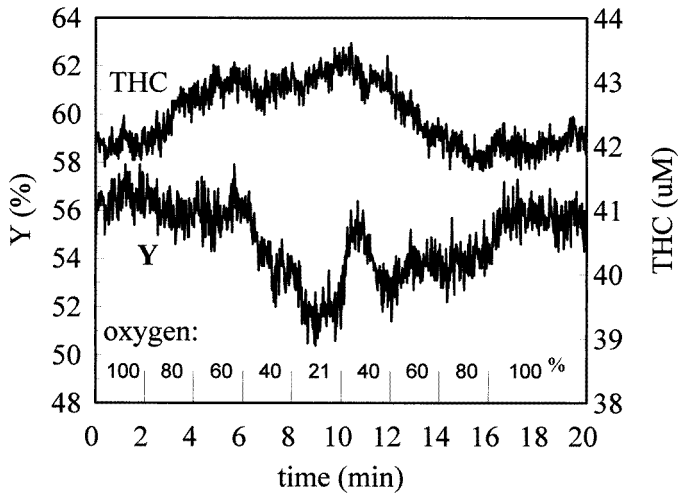

Figure 2. Time traces of the total haemoglobin concentration (THC) and saturation (Y) in the brain during a cyclic modulation of the inspired oxygen per cent as indicated in the figure.

corresponds to a decrease in arterial saturation from 99.9% to 97.7%, as measured by arterial blood gas analysis. A sequential change, first increase and then decrease, in cerebral saturation occurred during the time interval between 10 and 12 min. This was determined by a sudden decrease and subsequent recovery of the absorption coefficient at 758 nm, while the absorption coefficient at 830 nm did not show any particular feature at this time. The different behaviour of the absorption coefficient at two wavelengths leads us to believe that the peak in the saturation trace at times 10–12 min is not the result of an artefact of the optical measurement (because an artefact related to a movement of the piglet head or to the displacement of the optical probe is likely to affect the readings at the two wavelengths to a similar extent).

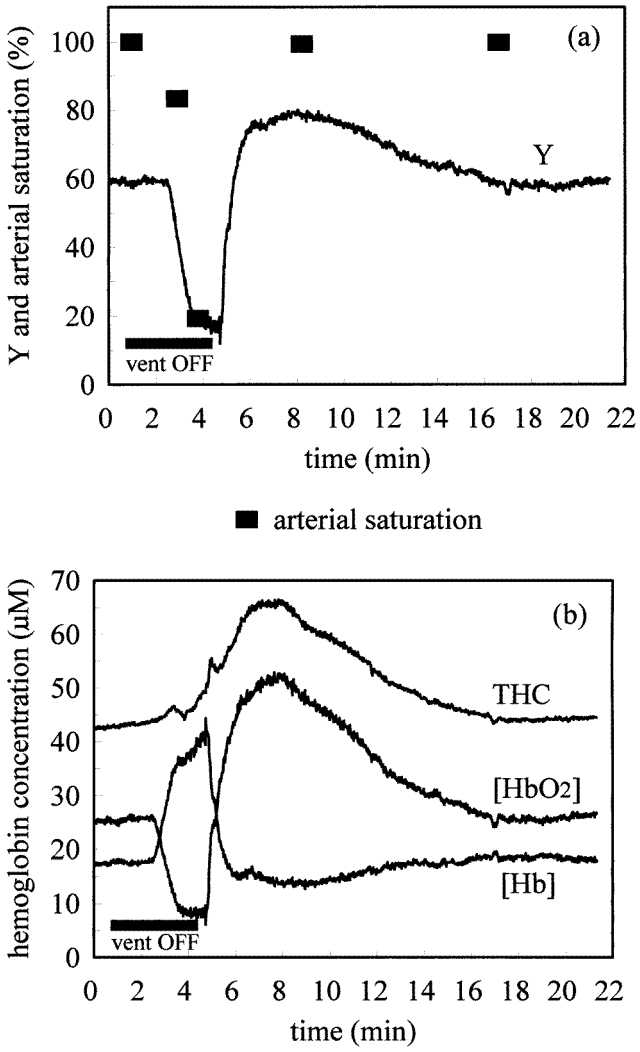

Figure 3. (*a*) Haemoglobin saturation in the brain (*Y*) and arterial saturation (SaO_2) during transient brain asphyxia. (*b*) Total haemoglobin concentration (THC), oxyhaemoglobin concentration ($[HbO_2]$) and deoxyhaemoglobin concentration ([Hb]) traces during transient brain asphyxia. In both panels, the black horizontal line indicates the time during which the ventilator was turned off.

3.4. Transient brain asphyxia

Figure 3 shows the cerebral haemoglobin saturation (panel (*a*)) and the concentrations of oxyhaemoglobin, deoxyhaemoglobin and total haemoglobin (panel (*b*)) recorded during transient brain asphyxia. The horizontal thick line in the figures indicates the period of asphyxia. As a result of asphyxia, we have recorded a strong decrease in haemoglobin saturation that reached a minimum value of $17 \pm 1\%$. After the resumption of the ventilation, the baseline tissue saturation recovered, after an evident overshoot (reperfusion phase), caused by the increase in cerebral blood flow carrying fully saturated arterial blood. An overshoot in the haemoglobin saturation during reperfusion has already been recorded by near-infrared spectroscopy in the brain of the piglet following asphyxia and hypotension (Stankovic *et al*

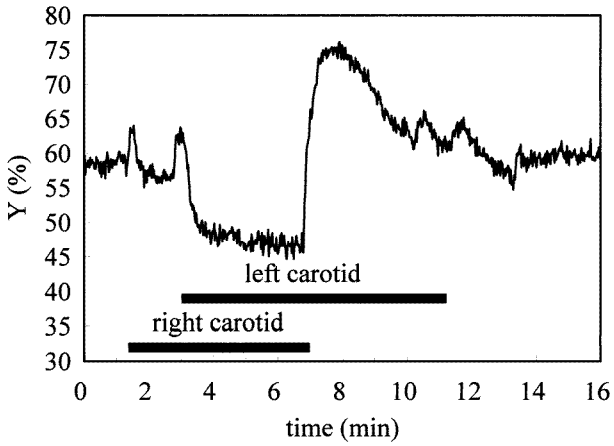

Figure 4. Brain haemoglobin saturation (Y) recorded during right and left carotid artery occlusion. The duration of the right and left occlusion is indicated in the figure.

1998), in the human brain after circulatory arrest (Smith *et al* 1990) and in the human muscle in response to pneumatic-cuff-induced forearm ischaemia (Hampson and Piantadosi 1988, Ferrari *et al* 1992, Fantini *et al* 1995). The symbols in figure 3(*a*) represent the oxygen saturation of the arterial blood drawn five times during the experiment. We note that the lowest arterial saturation (19.3%), where all of the tissue blood is likely to have a similar low value of oxygen saturation, is in excellent agreement with the corresponding tissue saturation value measured with the near-infrared tissue oximeter ($19 \pm 1\%$).

3.5. Carotid artery occlusion

Figure 4 shows the changes in cerebral saturation accompanying unilateral and bilateral carotid artery occlusion recorded by near-infrared spectroscopy. The two horizontal lines in the figure indicate the duration and the side of the occlusion. Figure 4 shows that the bilateral carotid occlusion causes a large drop in tissue saturation, as opposed to the small desaturation caused by unilateral occlusion. The peaks in the saturation trace at the times of clamping and release of the carotid arteries are tentatively assigned to piglet head movements that occurred during the placement of the vascular clamps.

3.6. Terminal brain asphyxia

Figure 5 shows the recorded traces of the optical coefficients (panel (*a*)) and the haemoglobin-related parameters (panel (*b*)) before and after piglet A was sacrificed. The marker (vertical line) in figure 5 indicates the time of the pentobarbital sodium IV injection. The absorption changes translate into a sudden decrease in the concentration of oxyhaemoglobin and the consequent drop in saturation that reaches a stable value of about $32.2 \pm 0.5\%$ after death. The reduced scattering coefficient started to decrease right after death. However, about 5 min after death, the reduced scattering coefficient inverted the trend starting to increase.

3.7. Optical monitoring of arterial pulsation and respiration

Figure 6(*a*) reports the time traces of the normalized dc intensity at a source–detector separation $r = 1.5$ cm, the normalized dc slope versus r (i.e. the slope of $\ln(r^2\mathrm{dc})$ measured at r ranging

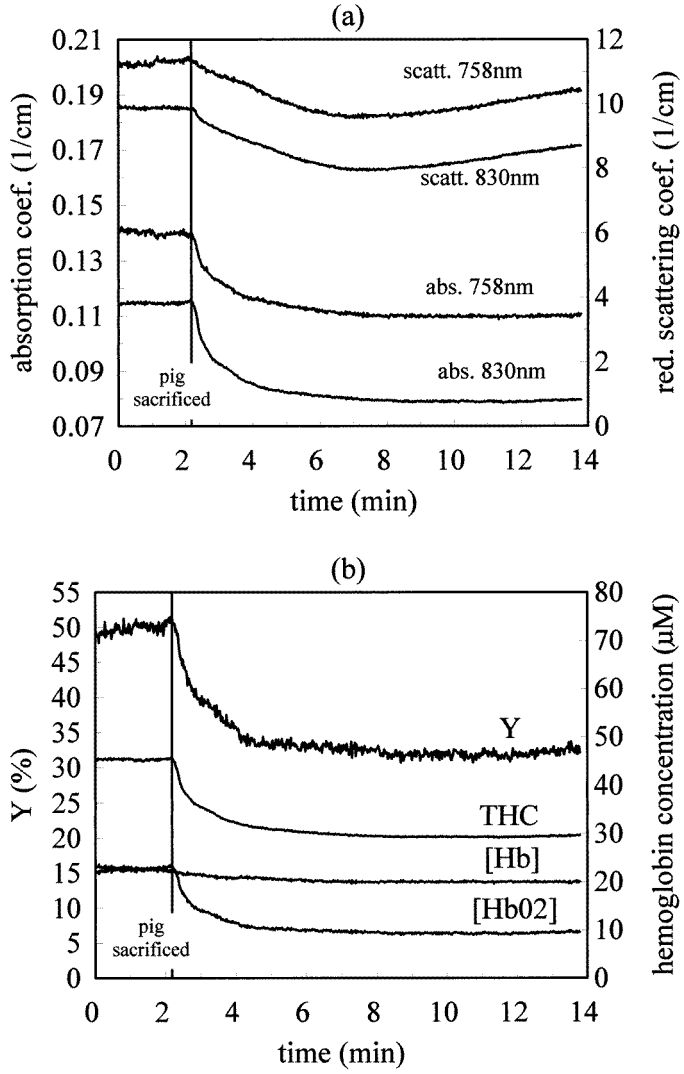

Figure 5. Time traces of the optical coefficients (abs. $= \mu_a$, scatt. $= \mu_s'$) (panel (*a*)) and the haemoglobin-related parameters (panel (*b*)) before and after the piglet is sacrificed.

from 1.5 to 3.0 cm) and the normalized absorption coefficient. The normalization has been performed by dividing each data point by the average value over the corresponding time trace. Figure 6(*b*) illustrates the fast Fourier transform (FFT) power spectra for the dc, dc slope and μ_a. The FFTs are computed on a total time interval of 82 s (512 data points) which is 3.4 times longer than the time interval reported in the x-axis of figure 6(*a*). Both figures 6(*a*) and 6(*b*) show the three cases listed in section 2.5, namely (a) piglet alive, ventilator on; (b) piglet dead, ventilator on and (c) piglet dead, ventilator off. The dc intensity, dc slope and absorption coefficient reported in figure 6 are all measured at 830 nm, where the oxyhaemoglobin-rich arterial blood shows a higher absorption than at 758 nm.

The heart rate of 131 ± 1 min^{-1} (as measured by pulse oximetry) is reflected in the arterial pulse recorded by the dc and dc slope, while it does not appear in the absorption trace.

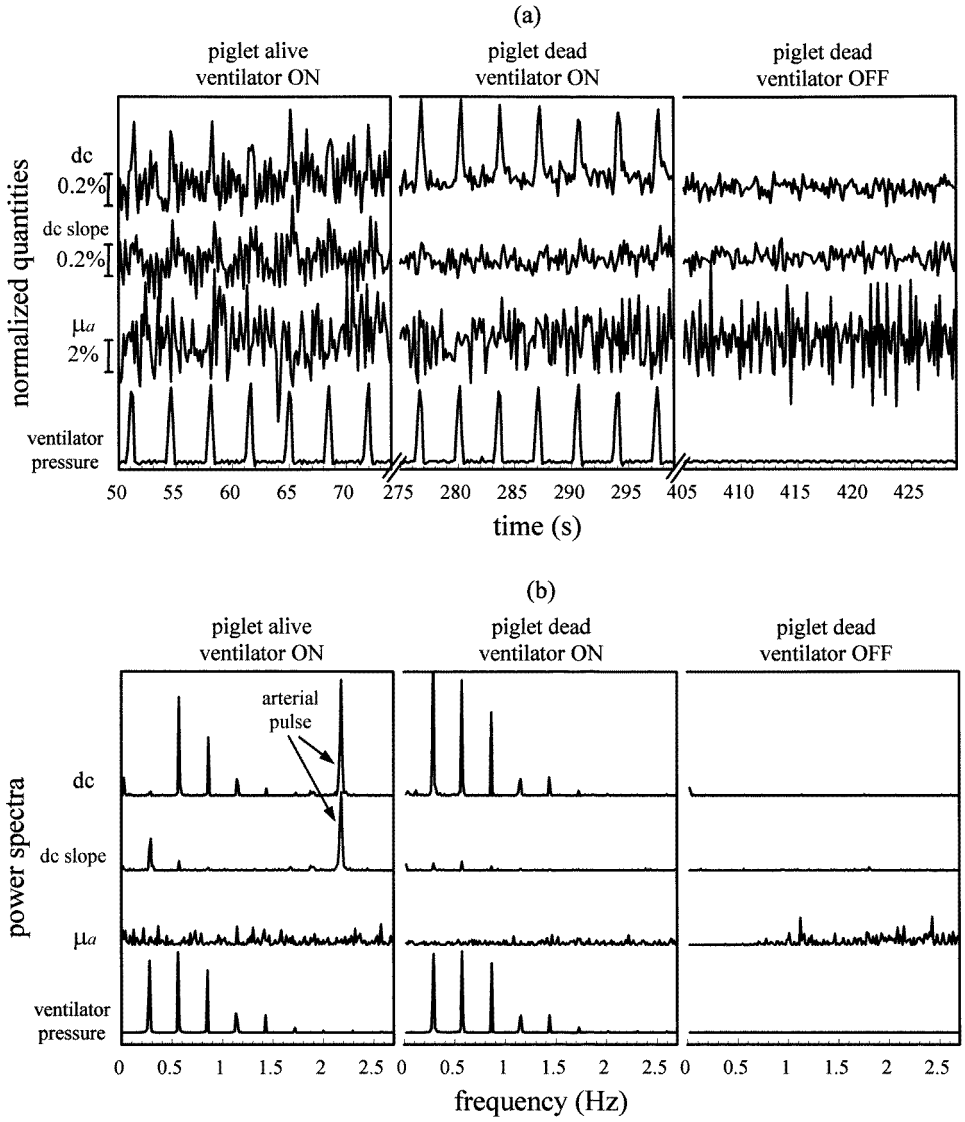

Figure 6. (*a*) Time traces of the normalized dc (at $r = 1.5$ cm), dc slope and μ_a at 830 nm under three conditions: (a) piglet alive, ventilator on; (b) piglet dead, ventilator on; (c) piglet dead, ventilator off. The ventilator pressure is also shown. The amplitude of the fluctuations in the dc, dc slope and μ_a are quantified by the vertical segments shown next to the left y-axis. (*b*) Power spectra of the four traces shown in part (*a*) under the same three conditions. The two peaks indicated by the arrows correspond to the arterial pulse.

The corresponding peaks in the dc and dc slope power spectra are centred at 2.18 Hz and are indicated by arrows in figure 6(*b*). The reason for the lack of detection of the arterial pulse in μ_a is the contribution of the phase noise (both the ac amplitude and the phase are used to calculate μ_a) which overcomes the arterial pulse signal. In other words, in the power spectrum of μ_a, the peak associated with the arterial pulse is buried within the noise and could be detected only by using longer (than 82 s) integration times. Equation (3) allows us to quantify

the change in μ_a corresponding to the dc change of about 0.2% associated with the heartbeat. Such a change in μ_a is about 0.0003 cm^{-1} or 0.2% (the average value of μ_a at 830 nm was 0.165 cm^{-1} in piglet C before sacrifice), which is less than the measurement precision in μ_a (see figure 5(*a*) and table 2). The pulse-induced change in μ_a obtained with the dc slope method (equation (11)) is larger, being equal to 0.0008 cm^{-1} at 830 nm and 0.0005 cm^{-1} at 758 nm. We observe that the ratio of the values of $\Delta\mu_a$ at the two wavelengths ($8/5 = 1.6$) is in excellent agreement with the ratio of the oxyhaemoglobin extinction coefficients at the same wavelengths ($\varepsilon^{830nm}_{HbO_2}/\varepsilon^{758nm}_{HbO_2} = 1.57$). This result supports the hypothesis that the pulsatile component measured in the brain originates from the arterial compartment (Mendelson 1992, Kohl *et al* 1998), even though more accurate spectral measurements are required to fully address this point. As expected, the peaks at the arterial pulse frequency in the power spectra of the dc and dc slope disappear after the piglet is sacrificed.

The respiration rate of 17 ± 1 min^{-1} corresponds to the fundamental Fourier component at 0.29 Hz which appears in the power spectrum of the airway pressure. This component is accompanied by its harmonics extending up to about 2 Hz as a result of the short duration of the pressure pulses ($\sim$1 s). The power spectrum of the dc intensity shows the fundamental component as well as the harmonics up to about 2 Hz. This means that the dc intensity records each respiration event with a fast response time, as confirmed by the sharp peaks in the time trace (figure 6(*a*)). Such a fast response suggests that the dc signal may be mostly affected by the respiratory motion, which can modify the optical fibre/skin coupling. That this is indeed the case is shown by the permanence of the respiration peaks in the dc power spectrum even after the pig was sacrificed. Even though the piglet head was immobilized within the stereotaxic instrument, we could observe a small respiration-related motion in the area closer to the neck of the animal. Apparently, such a slight motion can significantly affect the dc intensity trace. It is noteworthy that the fundamental frequency is weak in the dc power spectrum recorded with the piglet alive. This result indicates that the dc intensity is also recording a slower response to respiration. This slower response disappears after the piglet is sacrificed, so that the fundamental frequency becomes the dominant component.

The dc slope shows a different behaviour from the dc intensity recorded at one single location. The respiration signal can be seen in the dc slope, but the power spectrum shows a reduced number of harmonics, indicating a slower temporal response (also visible in figure 6(*a*)). This slower response is more likely to reflect physiological changes in the tissue. In fact, the respiration signal is significantly reduced in the dc slope after sacrifice. The reason for the different behaviour of the dc intensity and the dc slope is that a motion artefact that affects the dc at the four source–detector distances to a similar extent, will have little effect on the dc slope (Fantini *et al* 1995). In this particular case, we found that the respiratory motion strongly affects the dc at 1.5 cm, but has a little effect on the dc at 3.0 cm. This different influence on the dc data at the various distances accounts for the residual sensitivity of the dc slope to the respiratory motion. The respiration signal is not detected in the μ_a trace for the same reason that the arterial pulse is not detected. As expected, the power spectra of all optical data flattened out after the ventilator was turned off.

4. Discussion

4.1. Measurements of cerebral haemoglobin saturation

The haemoglobin saturation, defined as the fraction of haemoglobin that binds oxygen, depends on several factors such as the partial pressure of oxygen, body temperature, pH and 2,3-diphosphoglycerate (DPG) concentration. Under normal conditions, the partial pressure

of oxygen (P_{O_2}) and the haemoglobin saturation in arterial blood are about 95–96 mmHg and 97–98% respectively. The difference between the oxygen partial pressure in arterial blood (95–96 mmHg) and in tissues (<40 mmHg) determines the oxygen diffusion from the capillaries into the tissues. The capillary P_{O_2} falls to a value of about 40 mmHg, determining a venous saturation of about 75%. Therefore, under normal conditions at rest, the body consumes, on the average, only 25% of the haemoglobin-bound oxygen provided by the arterial blood. This consumption can be higher in individual organs, or under abnormal or non-rest conditions when metabolic demand is increased. For instance, the haemoglobin saturation of the internal jugular vein in 50 healthy young men (18 to 29 years of age) at rest was found to range between 55.3% and 70.7% (average 61.8%) (Gibbs *et al* 1942). In current clinical practice, jugular venous oxygen saturation, which might be a relevant clinical parameter for correlation with cerebral near-infrared spectroscopy, is considered to be normal in the range 55% to 75% (Lewis *et al* 1996).

It is assumed that near-infrared spectroscopy mostly probes smaller blood vessels, particularly arterioles, venules and capillaries (Liu *et al* 1995a). On the one hand this is a valuable feature because it allows one to obtain information about the oxygen saturation of the blood in the capillaries, where the diffusion-driven exchange of oxygen with the tissue occurs. In other words, tissue spectroscopy gives direct information about the oxygen supply and consumption at the particular tissue examined. On the other hand, since the haemoglobin in arterioles, venules and capillaries has a wide range of oxygen saturation values, it is not easy to validate the saturation values measured by tissue spectroscopy (Y) with those of either arterial (SaO_2) or venous (SvO_2) blood. In the literature one can find baseline values of optically measured cerebral haemoglobin saturation ranging from about 60% in human subjects (McCormick *et al* 1991, Sevick *et al* 1991, De Blasi *et al* 1995, Levy *et al* 1995), to 84% in piglets after removal of the scalp (Du *et al* 1998). We believe that this wide range of values is mostly determined by the measurement protocol and by the algorithm of data analysis, which may be affected in different ways by the strong tissue inhomogeneity. The relationship between the actual cerebral optical properties and the absolute values measured with near-infrared brain spectroscopy is still an open question, especially in the case of the adult human head. The small size of the scalp/skull layer in the newborn piglet may introduce a less significant error in quantitative, multidistance spectroscopy of the brain. However, a possible effect of the tissue inhomogeneity should be kept in mind when considering our measured values of cerebral haemoglobin saturation and concentration of 60% and 42 μM respectively. Nevertheless, our measurements give some indications about the significance of the absolute value of cerebral saturation. In fact, a direct comparison between tissue saturation and arterial saturation can be done at very low arterial oxygen saturation values, where it can be assumed that the haemoglobin in all three vascular compartments (arterial, venous and capillary) has a similar oxygen saturation level. Under this condition, during transient brain asphyxia, we found an excellent agreement between the absolute cerebral saturation (Y) measured with frequency-domain spectroscopy and arterial saturation (SaO_2) (see figure 3(*a*) toward the end of the period with the ventilator off). It should be noted that this agreement is even better than expected, since the error in the absolute value of Y is at least 6% (see table 2). Furthermore, the significant overshoot in cerebral saturation observed after transient brain asphyxia as well as after carotid occlusion leads us to believe that the measured baseline saturation should not be a significant underestimate of the actual regional cerebral saturation.

The different information content of cerebral haemoglobin saturation (Y) and SaO_2 is evident in our measurements during manipulations in the inspired oxygen concentration and during transient brain asphyxia. Figure 2 shows that the transition from 100% to 21% inspired oxygen concentration caused a decrease in cerebral haemoglobin saturation (Y) of 5%. Such a

decrease in Y corresponds to a decrease of 2.2% in SaO_2. This mismatch is an indication of the different nature of the cerebral saturation Y (which depends on a number of factors such as blood flow, oxygen consumption, vascularization, blood pooling, etc), and the arterial saturation SaO_2 (which is a systemic parameter determined by the efficiency of blood oxygenation in the lungs). In fact, the larger decrease in Y with respect to SaO_2 is the result of an increase in the cerebral concentration of deoxyhaemoglobin, which determines the increase in total haemoglobin concentration during low levels of inspired oxygen (see figure 2). The experiment on transient brain asphyxia reported in figure 3(*a*) also shows a significantly different behaviour of Y and SaO_2. Four minutes after the ventilation was re-established, the systemic arterial saturation was back to its baseline value of 99.9%. By contrast, near-infrared spectroscopy continued to record changes in cerebral haemoglobin saturation (Y) and blood volume for about 12 min after ventilation was re-established.

Figure 4 shows that a unilateral interruption in the carotid blood flow (right carotid artery clamp) does not significantly affect cerebral oxygenation. Bilateral carotid occlusion, however, caused a significant decrease in tissue perfusion. By removing the clamp from the right carotid artery (with the clamp on the carotid artery still in place), cerebral oxygenation fully recovered, reaching the baseline value after the usual overshoot. This experiment also demonstrates the capability of the collateral circulation to compensate significant haemodynamic perturbations affecting brain oxygenation.

4.2. Comparison of CW and frequency-domain measurements

Relative measurements performed with the DPF and dc slope methods are compared in figure 7, which shows the changes in oxyhaemoglobin concentration measured with the DPF method (at $r = 1.5$ and 3.0 cm) and with the dc slope method during the asphyxia protocol. During asphyxia (the period indicated as 'vent OFF' in figure 7), the DPF and dc slope curves are almost coincident and in good agreement with the frequency-domain multidistance method (shown as the thick line in figure 7). Such a good agreement can be explained by a lack of change in μ_s' (as we observed with the frequency-domain multidistance method) and by the fact that asphyxia is accompanied by a decrease in the heart rate, blood pressure and cerebral blood flow. Consequently, both the scalp and the brain were likely to be equally ischaemic, thus determining a spatially uniform desaturation of haemoglobin. By contrast, the DPF and dc slope curves split during the recovery period ($t > 6$ min in figure 7), which is in part due to the increase in μ_s' (by about 0.5 cm^{-1}) observed during the period of reperfusion. However, an increase in μ_s' should cause an overestimation of $\Delta\mu_a$, which is the case only for the dc slope method. The reason why the DPF method underestimates $\Delta\mu_a$ during the recovery may be related to the fact that single-distance methods are affected by changes occurring at thin superficial layers (such as the 2 mm thick skin/scalp layer), while multidistance methods performed at $r \geqslant 1.5$ cm are not. One should consider the possibility that the different vascular capacitance of the scalp (small capacitance) and the brain (large capacitance) might account for an inhomogeneous distribution of an increase in blood volume. This latter explanation would also account for the smaller value of $\Delta\mu_a$ measured with the DPF at $r = 1.5$ cm with respect to that measured at $r = 3.0$ cm (the traces obtained with the DPF at $r = 2.0$, 2.5 and 3.0 cm are almost coincident, so that only the one at 3.0 cm is shown in figure 7).

The analysis of the optical signals associated with the arterial pulse and respiration reported in figure 6, in conjunction with the measurement errors listed in table 2, gives valuable indications about the choice of the particular experimental approach in tissue spectroscopy. Depending on the particular application, one should find the best compromise among the

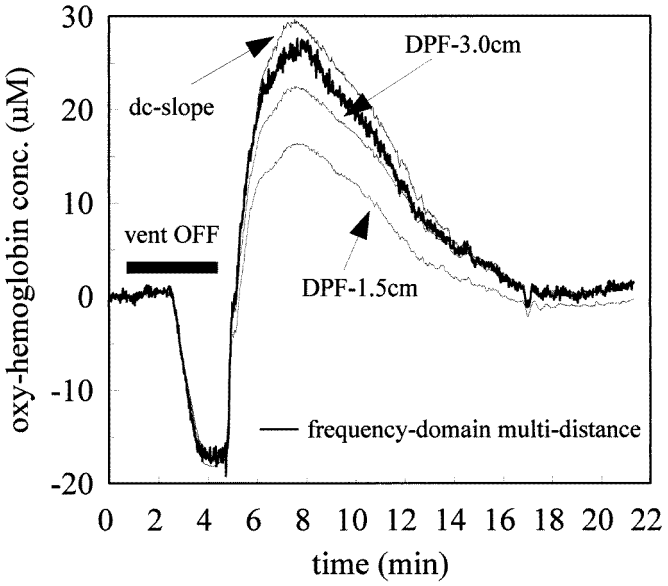

Figure 7. Changes in the oxyhaemoglobin concentration recorded during transient brain asphyxia (see also figure 3) with various non-invasive optical methods: (a) frequency-domain multidistance (thick line), (b) continuous-wave DPF with a source–detector separation of 1.5 cm (DPF-1.5cm) and 3.0 cm (DPF-3.0cm) and (c) continuous-wave dc slope.

advantages and disadvantages associated with the various approaches. For instance, the capability of frequency-domain spectroscopy to provide absolute readings (which was crucial in this study) comes at the expense of a reduced signal-to-noise ratio with respect to CW spectroscopy. If one is interested only in changes from baseline values, CW may be a better choice. However, table 1 (reproducibility errors) and figure 6 (case (b): when we kept the ventilator working after the death of the piglet) show that the single-distance CW data can be significantly affected by changes in the optical coupling with the skin and by motion artefacts. Furthermore, single-distance methods can be strongly affected by modifications occurring at a superficial layer rather than deep into the tissue. In some cases, a good compromise may be given by the dc slope, which provides a signal-to-noise ratio comparable to that of the dc intensity, without being so sensitive to motion artefacts, to the optical coupling and to the presence of superficial tissue layers.

4.3. Scattering changes after terminal asphyxia

Figure 5 is an example of a case where frequency-domain spectroscopy is required in order to separately measure the absorption and scattering properties of the brain tissue. In this case, the significant change in the reduced scattering coefficient would confound the measurements of $\Delta\mu_a$ performed with the DPF or dc slope methods. Previous studies have reported both a decrease (Yamashita *et al* 1996) and an increase (Du *et al* 1998) in the reduced scattering coefficient after death. We have observed an initial decrease in μ_s' immediately after death, followed by an increase in μ_s' occurring about 5 min after death. We believe that the initial decrease in the reduced scattering coefficient could be assigned to neural potassium depolarization as previously suggested by Chance *et al* (1997), whereas the later scattering increase could be associated with the biochemical and molecular changes accompanying cell

death (e.g. increase in intracellular Ca^{2+} and free fatty acids, loss of structural and functional integrity of the cellular osmotic barrier and loss of homeostasis and viability) (Kitagawa *et al* 1989). However, the investigation of the biochemical origin of these early and late scattering changes is beyond the scope of this study.

4.4. Number of animals

Per each measurement protocol, we have reported results obtained on only one piglet. The significance of these representative results is supported by (a) the precision and reproducibility (for repositioning of the optical probe) of our instrument (see table 2) and (b) the consistent results that we have found when some of the protocols were repeated on additional piglets. In particular, the reproducibility error in the saturation measurement (6%) is the key parameter to assess the significance of the agreement between Y and SaO_2 during asphyxia (figure 3(*a*)). The comparison between the CW and the frequency-domain measurements (figure 7) is relevant because the observed differences are much larger than the precision error (0.3 μM in $[HbO_2]$) of the measurement (table 2). The analysis of the optical signals associated with the respiration and the arterial pulsation is meaningful even if it is carried out on a single animal. In fact, the purpose of this analysis is to show the different effect of the respiratory motion on single-distance and multidistance measurements. In ten additional piglets, the baseline cerebral saturation and the total haemoglobin concentration have been confirmed to assume values in the range 50–60% and 40–50 μM respectively. The haemodynamic changes following death (see figure 5(*a*)) have been reproduced in two more piglets. In two additional cases, we observed a small (1–2 μM) increase in [Hb] after death. Finally, the scattering changes following death (initial decrease and successive increase) (figure 5(*a*)) have been reproduced in five more animals.

5. Conclusion

We have reported our results of non-invasive frequency-domain and continuous-wave (CW) spectroscopy on the piglet brain *in vivo*. We have analysed the CW data with the differential pathlength factor (DPF) approach and with a dc slope method. We observe that in this article the dc slope method has been used simply as an alternative CW approach to the DPF method, where μ_s' rather than the DPF is assigned a constant value. In the experiments where we have applied the dc slope method, however, μ_s' was not always a constant. The μ_s' changes during terminal asphyxia are shown in figure 5(*a*) and significant scattering changes ($\sim$7%) where also observed during transient brain asphyxia. The assumption of a constant μ_s' may be avoided by using a 'mixed' CW and frequency-domain approach, where the dc slope method is complemented by an update of μ_s' every 5–10 s. This hybrid approach would combine the high signal-to-noise ratio afforded by the intensity measurement, with the quantitative feature of intensity and phase measurements. In this 'mixed' approach, the only assumption is that μ_s' does not change on a time scale shorter than 5–10 s.

Using diffusion theory, we have derived a mathematical relationship between the tissue optical properties and the DPF. The DPF is independent of the source–detector distance r in an infinite geometry, whereas the DPF shows a significant r dependence at $r < 3.0$ cm in a semi-infinite geometry (where the source and the detector are placed on the tissue surface). Our mathematical treatment assumes tissue homogeneity. The r dependence of the DPF *in vivo* can additionally be influenced by tissue inhomogeneity. At the wavelengths employed by us (758 and 830 nm), we found DPF values ranging from 4.9 (at $r = 1.5$ cm) to 6.3 (at $r = 3.0$ cm) for the piglet head.

The value of any particular technique for tissue oxygenation and perfusion monitoring is not only determined by its sensitivity to detect changes, but also by its ability to provide different types of information (e.g. oxygenation, blood flow and volume, oxygen consumption, heart rate etc). Near-infrared spectroscopy can be a valuable non-invasive tool in monitoring cerebral haemodynamics and oxygenation *in vivo* as it provides information on cerebral perfusion and oxygenation that cannot be obtained by systemic arterial blood sampling. Frequency-domain spectroscopy provides quantitative readings of the absolute values of the haemoglobin concentration and saturation in the brain. In the presence of a relatively thin ($\lesssim$0.4 cm) scalp/skull layer (as in the case of the neonatal piglet), these absolute values of haemoglobin concentration and saturation should be actually representative of the brain. By contrast, the significantly thicker tissue inhomogeneities (skin, scalp, skull, dura, cerebrospinal fluid, convolutions of the brain etc) found in the adult human head have an effect on the absolute, non-invasive optical measurements that is still not fully characterized. Continuous-wave spectroscopy can quantify changes in the haemoglobin concentration, by assuming that the tissue scattering is a constant. A comparison of the absolute and relative measurements with the different techniques indicates that they are not equivalent when they are applied *in vivo*. We have discussed some of the parameters and approximations that characterize each approach to tissue spectroscopy. Based on the required precision and accuracy of a particular tissue-spectroscopy experiment, we have provided some guidance in the choice between the frequency-domain, continuous-wave, multidistance and single-distance approaches.

Acknowledgments

We thank Jean Handel, Darrin Chester, Pauline Bitteto and Patricia Johnson for their technical assistance. This research is supported in part by the US National Institutes of Health (NIH) grant no CA57032 and by Whitaker-NIH grant No RR10966.

References

Arridge S R, Cope M and Delpy D T 1992 The theoretical basis for the determination of optical pathlengths in tissue: temporal and frequency analysis *Phys. Med. Biol.* **37** 1531–60

Belardinelli R, Barstow T J, Porszasz J and Wasserman K 1995 Changes in skeletal muscle oxygenation during incremental exercise measured with near infrared spectroscopy *Eur. J. Appl. Physiol.* **70** 487–92

Brun N C, Moen A, Børch K, Saugstad O D and Greisen G 1997 Near-infrared monitoring of cerebral tissue oxygen saturation and blood volume in newborn piglets *Am. J. Physiol.* **273** H682–H686

Chance B, Dait M T, Zhang C, Hamaoka T and Hagerman F 1992 Recovery from exercise-induced desaturation in the quadriceps of elite competitive rowers *Am. J. Physiol.* **262** C766–C775

Chance B, Luo Q, Nioka S, Alsop D C and Detre J A 1997 Optical investigations of physiology: a study of intrinsic and extrinsic biochemical contrast *Phil. Trans. R. Soc.* B **352** 707–16

Cheatle T R, Potter L A, Cope M, Delpy D T, Coleridge Smith P D and Scurr J H 1991 Near-infrared spectroscopy in peripheral vascular disease *Br. J. Surg.* **78** 405–8

Cope M and Delpy D T 1988 System for long-term measurement of cerebral blood and tissue oxygenation in newborn infants by near infrared transillumination *Med. Biol. Eng. Comput.* **26** 289–94

Cope M, van der Zee P, Essenpreis M, Arridge A R and Delpy D T 1991 Data analysis methods for near infrared spectroscopy of tissues: problems in determining the relative cytochrome aa_3 concentration *Proc. SPIE* **1431** 251–63

De Blasi R A, Cope M, Elwell C, Safoue F and Ferrari M 1993 Non invasive measurement of human forearm oxygen consumption by near infrared spectroscopy *Eur. J. Appl. Physiol.* **67** 20–5

De Blasi R A, Fantini S, Franceschini M A, Ferrari M and Gratton E 1995 Cerebral and muscle oxygen saturation measurement by frequency-domain near infra-red spectrometer *Med. Biol. Eng. Comput.* **33** 228–30

De Blasi R A, Ferrari M, Natali A, Conti G, Mega A and Gasparetto A 1994 Noninvasive measurement of forearm blood flow and oxygen consumption by near-infrared spectroscopy *J. Appl. Physiol.* **76** 1388–93

Delpy D T, Cope M, van der Zee P, Arridge S, Wray S and Wyatt J 1988 Extimation of optical pathlength through tissue from direct time of flight measurement *Phys. Med. Biol.* **33** 1433–42

Du C, Andersen C and Chance B 1998 Quantitative detection of hemoglobin saturation on piglet brain by near-infrared frequency-domain spectroscopy *Proc. SPIE* **3194** 55–62

Eaton W A, Hanson L K, Stephens P J, Sutherland J C and Dunn J B R 1978 Optical spectra of oxy- and deoxyhemoglobin *J. Am. Chem. Soc.* **100** 4991–5003

Edwards A D, Richardson C, Van der Zee P, Elwell C, Wyatt J S, Cope M, Delpy D T and Reynolds E O R 1993 Measurement of hemoglobin flow and blood flow by near-infrared spectroscopy *J. Appl. Physiol.* **75** 1884–9

Edwards A D, Wyatt J S, Richardson C, Potter A, Delpy D T, Cope M and Reynolds E O R 1988 Cotside measurement of cerebral blood flow in ill newborn infants by near infrared spectroscopy *Lancet* **ii** 770–1

Elwell C E, Cope M, Edwards A D, Wyatt J S, Delpy D T and Reynolds E O R 1994 Quantification of adult cerebral hemodynamics by near-infrared spectroscopy *J. Appl. Physiol.* **77** 2753–60

Essenpreis M, Elwell C E, Cope M, van der Zee P, Arridge S R and Delpy D T 1993 Spectral dependence of temporal point spread functions in human tissues *Appl. Opt.* **32** 418–25

Fantini S, Franceschini M A, Fishkin J B, Barbieri B and Gratton E 1994a Quantitative determination of the absorption spectra of chromophores in scattering media: a light-emitting-diode based technique *Appl. Opt.* **33** 5204–13

Fantini S, Franceschini M A and Gratton E 1994b Semi-infinite-geometry boundary problem for light migration in highly scattering media: a frequency-domain study in the diffusion approximation *J. Opt. Soc. Am.* B **11** 2128–38

Fantini S, Franceschini M A, Maier J S, Walker S A, Barbieri B and Gratton E 1995 Frequency-domain multichannel optical detector for non-invasive tissue spectroscopy and oximetry *Opt. Eng.* **34** 32–42

Farrel T J, Patterson M S and Wilson B 1992 A diffusion theory model of spatially resolved, steady-state diffuse reflectance for the noninvasive determination of tissue optical properties *in vivo Med. Phys.* **19** 879–88

Ferrari M, Wei Q, Carraresi L, de Blasi R and Zaccanti G 1992 Time-resolved spectroscopy of the human forearm *J. Photochem. Photobiol.* B **16** 141–53

Franceschini M. A, Fantini S and Gratton E 1994 LEDs in frequency domain spectroscopy of tissues *Proc. SPIE* **2135** 300–6

Franceschini M A *et al* 1998a Quantitative near-infrared spectroscopy on patients with peripheral vascular disease *Proc. SPIE* **3194** 112–15

Franceschini M A, Fantini S, Paunescu L A, Maier J S and Gratton E 1998b Influence of a superficial layer in the quantitative spectroscopic study of strongly scattering media *Appl. Opt.* **37** 7447–58

Franceschini M. A, Wallace D, Barbieri B, Fantini S, Mantulin W W, Pratesi S, Donzelli G P and Gratton E 1997 Optical study of the skeletal muscle during exercise with a second generation frequency-domain tissue oximeter *Proc. SPIE* **2979** 807–14

Gibbs E L, Lennox W G, Nims L F and Gibbs F A 1942 Arterial and cerebral venous blood—arterial-venous difference in man *J. Biol. Chem.* **144** 325–32

Gopinath S P, Robertson C S, Grossman R G and Chance B 1993 Near-infrared spectroscopic localization of intracranial hematomas *J. Neurosurg.* **79** 43–7

Gratton G, Corballis P M, Cho E, Fabiani M and Hood D C 1995 Shades of gray matter: noninvasive optical images of human brain responses during visual stimulation *Psychophysiology* **32** 505–9

Hamaoka T, Iwane H, Shimomitsu T, Katsumura T, Murase N, Nishio S, Osada T, Kurosawa Y and Chance B 1996 Noninvasive measures of oxidative metabolism on working human muscles by near-infrared spectroscopy *J. Appl. Physiol.* **81** 1410–17

Hampson N B and Piantadosi C A 1988 Near infrared monitoring of human skeletal muscle oxygenation during forearm ischemia *J. Appl. Physiol.* **64** 2449–57

Hennes H J, Richter B, Lott C, Dick W, Boor S and Hanley D F 1999 Follow-up in patients with subdural haematomas using near-infrared spectroscopy (NIRS) *Proc. SPIE* **3566** 182–92

Homma S, Eda H, Ogasawara S and Kagaya A 1996 Near-infrared estimation of O_2 supply and consumption in forearm muscles working at varying intensity *J. Appl. Physiol.* **80** 1279–84

Kitagawa K *et al* 1989 Microtubule-associated protein 2 as a sensitive marker for cerebral ischemic damage—immunohistochemical investigation of dendritic damage *Neuroscience* **31** 401–11

Kohl M, Nolte C, Heekeren H R, Horst S, Scholz U, Obrig H and Villringer A 1998 Changes in cytochrome-oxidase oxidation in the occipital cortex during visual stimulation: improvement in sensitivity by the determination of the wavelength dependence of the differential pathlength factor *Proc. SPIE* **3194** 18–27

Kooijman H M, Hopman M T E, Colier W N J M, van der Vliet J A and Oeseburg B 1997 Near infrared spectroscopy for noninvasive assessment of claudication *J. Surg. Res.* **72** 1–7

Levy W J, Levin S and Chance B 1995 Near-infrared measurement of cerebral oxygenation *Anesthesiology* **83** 738–46

Lewis S B, Myburg J A, Thornton E L and Reilly P L 1996 Cerebral oxygenation monitoring by near-infrared spectroscopy is not clinically useful in patients with severe closed-head injury: a comparison with jugular venous bulb oximetry *Crit. Care Med.* **24** 1334–8

Liu H, Boas D A, Zhang Y, Yodh A G and Chance B 1995b A simplified approach to characterize optical properties and blood oxygenation in tissue using continuous near infrared light *Proc. SPIE* **2389** 496–502

Liu H, Hielscher A H, Beauvoit B, Wang L, Jacques S L, Tittel F K and Chance B 1995a Near infrared spectroscopy of a heterogeneous, turbid system containing distributed absorber *Proc. SPIE* **2326** 164–72

McCormick P W, Stewart M, Goetting M G, Dujovny M, Lewis G and Ausman J I 1991 Noninvasive cerebral optical spectroscopy for monitoring cerebral oxygen delivery and hemodynamics *Crit. Care Med.* **19** 89–97

McCully K K, Halber C and Posner J D 1994 Exercise-induced changes in oxygen saturation in the calf muscles of elderly subjects with peripheral vascular disease *J. Gerontol. Biol. Sci.* **49** B128–B134

Meek J H, Elwell C E, Khan M J, Romaya J, Wyatt J S, Delpy D T and Zeki S 1995 Regional changes in cerebral haemodynamics as a result of a visual stimulus measured by near infrared spectroscopy *Proc. R. Soc.* B **261** 351–6

Mendelson Y 1992 Pulse oximetry: theory and applications for noninvasive monitoring *Clin. Chem.* **38** 1601–7

Millikan G A 1942 The oximeter, an instrument for measuring continuously the oxygen saturation of arterial blood in man *Rev. Sci. Instrum.* **13** 434–44

Miwa M, Ueda Y and Chance B 1995 Development of a time resolved spectroscopy system for quantitative non-invasive tissue measurement *Proc. SPIE* **2389** 142–9

Patterson M S, Andersson-Engels S, Wilson B C and Osei E K 1995 Absorption spectroscopy in tissue-simulating materials: a theoretical and experimental study of photon paths *Appl. Opt.* **34** 22–30

Patterson M S, Chance B and Wilson B C 1989 Time resolved reflectance and transmittance for the non-invasive measurement of optical properties *Appl. Opt.* **28** 2331–6

Quaresima V, Franceschini M A, Fantini S, Gratton E and Ferrari M 1998 Difference in leg muscles oxygenation during treadmill exercise by a new near infrared frequency-domain oximeter *Proc. SPIE* **3194** 116–20

Sahlin K 1992 Non-invasive measurements of O_2 availability in human skeletal muscle with near-infrared spectroscopy *Int. J. Sports and Med.* **13** 157–60

Sevick E M, Chance B, Leigh J, Nioka S and Maris M 1991 Quantitation of time- and frequency-resolved optical spectra for the determination of tissue oxygenation *Anal. Biochem.* **195** 330–51

Smith D S, Levy W, Maris M and Chance B 1990 Reperfusion hyperoxia in the brain after circulatory arrest in humans *Anesthesiology* **73** 12–19

Stankovic M R, Fujii A, Maulik D, Boas D, Kirby D and Stubblefield P G 1998 Optical monitoring of cerebral hemodynamics and oxygenation in the neonatal piglet *J. Matern. Fetal Invest.* **8** 71–8

Tamura M, Hoshi Y and Okada F 1997 Localized near-infrared spectroscopy and functional optical imaging of brain activity *Phil. Trans. R. Soc.* B **352** 737–42

Van der Zee P, Cope M, Arridge S R, Essenpreis M, Potter L A, Edwards A D, Wyatt J S, McCormick D C, Roth S C, Reynolds E O R and Delpy D T 1992 Experimentally measured optical pathlengths for the adult head, calf and forearm and the head of the newborn infants as a function of inter optode spacing *Adv. Exp. Med. Biol.* **316** 143–53

Villringer A and Chance B 1997 Non-invasive optical spectroscopy and imaging of human brain function *Trends Neurosci.* **20** 435–42

Wenzel R, Obrig H, Ruben J, Villringer K, Thiel A, Bernarding J, Dirnagl U and Villringer A 1996 Cerebral blood oxygenation changes induced by visual stimulation in humans *J. Biomed. Opt.* **1** 399–404

Wyatt J S, Cope M, Delpy D T, van der Zee P, Arridge S R, Edwards A D and Reynolds E O R 1990 Measurement of optical pathlength for cerebral near infrared spectroscopy in newborn infants *Dev. Neurosci.* **12** 140–4

Yamashita Y, Oda M, Naruse H and Tamura M 1996 *In vivo* measurement of reduced scattering coefficient and absorption coefficient of living tissue using time-resolved spectroscopy *OSA Trends in Optics and Photonics on Advances in Optical Imaging and Photon Migration* vol 2, ed R R Alfano and J G Fujimoto (Washington, DC: Optical Society of America) pp 387–90